

Resource Allocation in Cell-Free MU-MIMO Multicarrier System with Finite and Infinite Blocklength

Jiafei Fu, Pengcheng Zhu, *Member, IEEE*, Bo Ai, *Fellow, IEEE*,
Jiangzhou Wang, *Fellow, IEEE*, Xiaohu You, *Fellow, IEEE*

Abstract—The explosive growth of data in the next generation mobile communications results in more scarce spectrum resources. It is important to optimize the system performance under limited resources. In this paper, we investigate how to achieve weighted throughput (WTP) maximization for cell-free (CF) multiuser MIMO (MU-MIMO) multicarrier (MC) systems through resource allocation (RA), in the cases of finite blocklength (FBL) and infinite blocklength (INFBL) regimes. To ensure the quality of service (QoS) of each user, particularly for the block error rate (BLER) and latency in the FBL regime, the WTP gets maximized under the constraints of total power consumption and required QoS metrics. Since the channels vary in different subcarriers (SCs) and inter-user interference strengths, the WTP can be maximized by scheduling the best users in each time-frequency (TF) resource and advanced beamforming design, while the resources can be fully utilized. With this motivation, we introduce a 0-1 scheduling indication variable to represent whether the user is selected on the current TF resource. However, the problem mentioned above is a mixed integer nonlinear programming (MINLP) problem that is challenging to address due to the integer scheduling indication variable and the beamforming vector. Therefore, we propose a nested iteration algorithm to solve this highly non-convex problem, where the user scheduling (US) scheme is optimized by gene-aided (GA) algorithm in the outer iteration, while the successive convex approximation (SCA) is used for beamforming design in inner iteration. Simulation results demonstrate that the proposed MU-MIMO scheduling scheme outperforms the other two traditional scheduling schemes, including single-user MIMO (SU-MIMO) and full-user MIMO (FU-MIMO) RA schemes that may not necessarily be optimal. And the CF system in our scenario is capable of achieving higher spectral efficiency (SE) than the centralized antenna systems (CAS).

Index Terms—Cell-free (CF), Multiuser MIMO (MU-MIMO), Multicarrier (MC), finite blocklength (FBL), infinite blocklength (INFBL), Single-user MIMO (SU-MIMO), Full-user MIMO (FU-MIMO), Successive convex approximation (SCA), Gene-aided (GA), Centralized antenna systems (CAS).

I. INTRODUCTION

TO meet the requirements of the explosive growth of the future mobile communication services, researchers

focused on the research and development of the next generation mobile communications to achieve global coverage and interconnection of all things. Technologies with higher rates, wider coverage, higher connection density, ultra-reliability, and low-latency (URLLC) are studied and developed [1], so as to satisfy the various needs of communication services for vertical applications, such as autonomous driving, factory automation, and remote surgery [2], [3].

Cell-free (CF) as a novel cellular architecture without cell boundary can provide consistent services for all users with coordinated multipoint (CoMP) transmission [4], [5]. In cell-free systems, multiple access points (APs) connected to a central processor unit (CPU) in a baseband pool (BBP) through a wireless backhaul link or optical fiber collaboratively transmit signals to all users. The channel state information (CSI) is shared among the APs. Data-sharing and compression strategies are two commonly used transmission strategies to account for the limited backhaul capacity. For the data-sharing, APs cooperatively transmit the beamformed signals formed locally to the users. For the compression, the beamforming operation is performed in BBP first. The CPU compresses and forwards the beamformed signals to the APs, where compression is needed due to finite backhaul capacity. The extra DoF offered by distributed antenna cooperation can improve the spectral efficiency significantly [6]. Besides, the distance between APs and equipment becomes closer, reducing the transmission latency. Hence, CF is a potential paradigm that can be applied in short-packet transmission to enhance ultra-reliability and low-latency communications (URLLC).

The short-packet structure is considered as the typical frame structure in URLLC to realize the stringent requirements of 100us latency and 10^{-6} block error rate (BLER) [7], which is different from the Shannon theory where BLER and the packet length are assumed to be infinitely small and large [8], respectively. In [9], the tight approximation of the maximal achievable rate was first obtained by Polyanskiy at a given blocklength and the block error rate, which characterizes the relationship among rate, blocklength, and block error rate. This groundbreaking research has laid the foundation for the short-packet communication theory, thereby providing technical support for vertical industry applications. Yang in [10] further established achievability and converse bounds on the maximal achievable rate in quasi-static MIMO fading channels. According to the characteristics of short-packet communications [10]–[12], the outage probability concept considering both security

Jiafei Fu, Pengcheng Zhu and Xiaohu You are with National Mobile Communications Research Laboratory, Southeast University, Nanjing 210096, China. (e-mails: fujfei@seu.edu.cn; p.zhu@seu.edu.cn; xhyu@seu.edu.cn). Bo Ai is with the State Key Laboratory of Rail Traffic Control and Safety, Beijing Jiaotong University, Beijing 100044, China. (e-mail: boai@bjtu.edu.cn). Jiangzhou Wang is with the School of Engineering, University of Kent, CT2 7NZ Canterbury, U.K. (e-mail: j.z.wang@kent.ac.uk). Corresponding author: Pengcheng Zhu.

and reliability with an eavesdropper was proposed in [14], while effective outage capacity was further established as the performance metric to evaluate the security and reliability. The author in [15] studied the average secure block error rate of the downlink NOMA system in consideration of short-packet communications in flat Rayleigh fading channels. Besides, the author in [13] investigated the energy efficiency (EE) for non-orthogonal multiple access (NOMA) massive machine-type communication (mMTC) networks by optimizing the subchannel and power control, where sporadic and low-rate short-packet were used for information exchange among mMTC devices. As the number of users increases, how to satisfy the QoS of each user in mMTC with limited resources is still an open problem.

Fortunately, multicarrier transmission (MCT) (e.g., orthogonal frequency division multiple access (OFDMA)) is applied to guarantee high data rate transmission due to its flexibility for resources allocation, its resistance to multi-path fading and its ability to realize the multi-user diversity [16]–[18]. The author in [19] studied the resource allocation in multiple-input single-output (MISO) multicarrier (MC) NOMA systems, in which a full-duplex (FD) base station serves multiple half-duplex (HD) uplink and downlink users on the same subcarrier simultaneously, to maximize the WTP. An optimal power and subcarrier allocation scheme was proposed in [20] to provide a good balance between improving the system throughput and maintaining fairness among users. Compared to the traditional single-user MIMO (SU-MIMO) [21] in MCT systems that only one best user is likely to be served at each time-frequency resource and may not be able to fully utilize the system resources, MU-MIMO in MCT systems can provide additional degrees of freedom (DoF) to obtain diversity and multiplexing gains, where multiple single-antenna users are served by a transmitter equipped with a large number of antennas [22]–[25].

To this end, the author in [26] investigated three optimization problems regarding the weighted sum rate maximization, EE maximization, and user fairness problems by beamforming design for the downlink multiuser URLLC system, in which spatial multiplexing gain at the base station can be achieved without the need for multiple-antenna users. In [27], the author proposed a low-complexity algorithm to optimize the beamformer and the remote radio unit selection for improving the EE of a distributed massive MIMO multiuser system. However, since all users are scheduled in each time-frequency resource (Here, we define this type of multiuser scheduling MIMO as full-user MIMO (FU-MIMO)), these MC systems do not have user scheduling (US) operations actually. Since the channel fading coefficients at different subcarriers are statistically independent for different users, the maximal capacity can be obtained by choosing the best users for each subcarrier and allocating the corresponding transmitting power.

In order to investigate the user scheduling gain in MU-MIMO system, some studies have been carried out related to both resource allocation and multi-user scheduling in each subcarrier. The author in [28] explored joint uplink-downlink resource allocation for multi-user OFDMA-URLLC in mobile edge computing (MEC) systems. The problem regarding the

minimization of the total weighted power consumption of the system was studied under the constraint of the end-to-end delay of a computation task of each user. [29] formulated an optimization problem for maximizing the weighted system sum throughput while guaranteeing the QoS of the URLLC users in intelligent reflecting surface (IRS) enhanced URLLC multicell networks with OFDM access. Cheng researched a robust resource block assignment and beamforming design problem for minimizing the total transmit power of the central controller in OFDMA-URLLC system about the worst-case SNR while guaranteeing URLLC requirements [30]. As shown in [31], the network utility maximization problem is considered by optimizing the power vector and user selection for SU-MIMO and MU-MIMO in a coordinated massive MIMO system. The author in [32] constructed a joint system throughput and user rate satisfaction problem in CF massive MIMO systems. A dynamic user scheduling algorithm was proposed to adjust the list and number of paired users according to the channel quality and transmission requirements of users.

However, the aforementioned studies usually concentrate on joint user scheduling and resource allocation in multi-cell or single base station scenarios [33]–[35]. Most papers discussed resource allocation while full-user scheduling is considered to obtain diversity gain in CF massive MIMO system. Few works paid attention to CF MU-MIMO resource allocation. Therefore, we allocate the resources in CF MU-MIMO MC systems with both infinite blocklength (INFB) and finite blocklength (FBL). The centralized antenna system (CAS) is also investigated as the comparison scheme. Different from the single-user scheduling and full-user scheduling scenarios, we investigate the weighted throughput (WTP) in terms of the multi-user scheduling and the beamforming design in CF systems. In the sequel, we propose a nested iterative algorithm named USBDA to solve an MINLP problem. Furthermore, a two-stage algorithm is used for the USBDA to reduce the computational complexity. The main contributions of this work are listed below.

- We consider a WTP maximization problem in a CF MU-MIMO MC system by optimizing the user scheduling scheme and the beamforming vector while satisfying the constraints of the total power consumption and the minimum QoS of each user with given TF resources and BLER. The CAS is investigated as the comparison scheme of CF systems in our proposed scenarios. And the WTP maximization problem is applied in both INFB and FBL regimes.
- By beamforming design and scheduling the multiple best users according to the channel condition in different frequency resources, the WTP can be maximized and the limited resources can be fully utilized in MU-MIMO scenario compared to the traditional resource allocation in SU-MIMO and FU-MIMO scenarios. The user scheduling optimization problem is transformed to optimize a 0-1 scheduling indication variable that represents whether the user is scheduled on the current time-frequency resource. Hence each user's blocklength equals the sum of its corresponding scheduling indication variables in the total

radio resources.

- A nested iterative algorithm named USBDA is proposed to solve the WTP maximization problem both in FBL and INFBL regimes respectively. The inner iteration is the beamforming design, and the gene-aided (GA) algorithm in the outer iteration is proposed for user scheduling optimization. Two-stage algorithm is proposed for the USBDA algorithm to reduce the computational complexity. For the first stage, the linear minimum mean square error (MMSE) beamformer rather than the proposed beamformer is used in the USBDA algorithm to obtain a preferable initial value of the US scheme. Hence, fewer generations are needed in the USBDA algorithm with the proposed beamformer in the second stage. Simulation results verify this advantage.

The rest of this paper is organized as follows. Section II describes the system model and formulates the WTP expression in CF MU-MIMO MC system both in INFBL regime and FBL regime with given block error rate. Section III and IV illustrate the solutions in INFBL and FBL regimes to solve the maximization problem of the WTP by optimizing the user scheduling scheme and the beamformer, respectively. And the proposed problem is applied to CAS in Section IV. Numerical results are given in Section V to compare the difference between CAS and CF systems. And demonstrate the effectiveness of the proposed MU-MIMO resource allocation scheme compared to its counterparts. Section VI concludes this paper.

Notation: Boldface lower-case letter, boldface upper-case letter, and lower-case letter represent a vector, matrix, and scalar respectively. $(\cdot)^T$, $(\cdot)^H$ denotes the transpose and the conjugate transpose. The expectation and the trace operation are denoted as $\mathbb{E}\{\cdot\}$ and $\text{Tr}\{\cdot\}$ respectively. Calligraphy letters \mathcal{M} are used to denote sets. And $|\mathcal{M}|$ represents the cardinality of the set \mathcal{M} . $\text{Re}\{\cdot\}$ is the operation to obtain the real part of a complex. $\|\cdot\|_0$ represents the operation of ℓ_0 -norm. $\langle A, B \rangle = A^H B$.

II. SYSTEM MODEL

In this section, we consider the downlink transmission process with compression transmission strategy in CF MU-MIMO MC system. Multi-users are scheduled in time-frequency resources according to three scheduling methods. Based on the user scheduling model, we formulate the downlink transmission signals received by different users. To this end, the WTP of the CF system both in the FBL regime and the INFBL regime are derived.

A. Compression Transmission Strategy

In Fig. 1, N APs are connected to a BBP in a CF system, hence the channel state informations are shared among all APs and the BBP. Each AP is equipped with M antennas, K single antenna users are distributed in a wide area. We denote that $\mathcal{N} = \{1, \dots, N\}$, $\mathcal{K} = \{1, \dots, K\}$. Different from the data-sharing transmission strategy that the information precoding is operated in local (i.e., in AP), in compression transmission strategy, information symbols ($s_k, \forall k \in \mathcal{K}$) of

users ($\text{UE}_k, \forall k \in \mathcal{K}$) are first centrally precoded for different APs by the CPU in the baseband pool. After that, the precoded symbols are combined according to their corresponding AP. Hence, we can denote the combined signal for $\text{AP}_n, \forall n \in \mathcal{N}$ as follow.

$$\bar{\mathbf{x}}_n = \sum_{k=1}^K \mathbf{w}_{kn} s_k, \quad (1)$$

where $\mathbf{w}_{kn} \in \mathbb{C}^{M \times 1}$ is the beamforming vector of AP_n and UE_k . And s_k is the normalized information symbol, i.e., $\mathbb{E}[|s_k|^2] = 1$.

Afterward, CPU forwards the compressed signals to their corresponding AP. The received signal in AP_n is expressed as

$$\mathbf{x}_n = \bar{\mathbf{x}}_n + \mathbf{e}_n, \quad (2)$$

where $\mathbf{e}_n \in \mathbb{C}^{M \times 1}$ is the quantization noise distributed as the Gaussian distribution with variance σ_e^2 , which is introduced by signal compression.

B. User Scheduling Schemes

In the downlink signal transmission stage, APs collaboratively transfer the compressed signals to the scheduled users on the time-frequency resource block (RB), which has F subcarriers and T time slots, a total of $T \times F$ resource elements (REs). Three user scheduling schemes are illustrated in Fig. 2. The detailed explanation of each user scheduling scheme is listed as

- RA-SU-MIMO (Fig. 2(a): resource allocation of single-user MIMO): up to one user is scheduled in each RE, indicating no interference between users.
- RA-FU-MIMO (Fig. 2(b): resource allocation of full-user MIMO): in each RE, all users are scheduled, which means no user scheduling operation at all.
- RA-MU-MIMO (Fig. 2(c): resource allocation of multi-user MIMO): multiple users are scheduled based on the channel conditions in each RE to maximize the system performance.

We point out that RA-MU-MIMO scheme includes the other two schemes. Namely, RA-SU-MIMO and RA-FU-MIMO schemes are two special cases of RA-MU-MIMO scheme. Therefore, we analyze the downlink signal transmission process based on the RA-MU-MIMO scheme. In each RE, we denote the transmitting beamforming vector of UE_k as $\mathbf{w}_k^{tf} = [(\mathbf{w}_{k1}^{tf})^H, \dots, (\mathbf{w}_{kN}^{tf})^H]^H, \forall \{t, f\} \in \{\mathcal{T}, \mathcal{F}\}, \mathcal{T} = \{1, \dots, T\}, \mathcal{F} = \{1, \dots, F\}$, and $\mathbf{w}_{kn}^{tf} \in \mathbb{C}^{M \times 1}, \forall n \in \mathcal{N}$ is the beamforming vector between AP_n and UE_k . Hence, the transmitting signal in time slot t and subcarrier f is expressed as

$$\mathbf{x}^{tf} = \sum_{k \in \mathcal{K}} \mathbf{w}_k^{tf} s_k^{tf} + \mathbf{e}^{tf}, \quad (3)$$

where s_k^{tf} is the normalized information symbol of UE_k in time slot t and subcarrier f , i.e., $\mathbb{E}[|s_k^{tf}|^2] = 1$. $\mathbf{e}^{tf} = [\mathbf{e}_1^{tf}, \dots, \mathbf{e}_N^{tf}]^H$ is the quantization noise vector transmitted from all the N APs. If $\mathbf{w}_k^{tf} = \mathbf{0}$ represents UE_k is not scheduled, and vice versa.

In each RE, we denote the channel fading coefficient of UE_k as $\mathbf{h}_k^{tf} = [(\mathbf{h}_{k1}^{tf})^H, \dots, (\mathbf{h}_{kN}^{tf})^H]^H$, where $\mathbf{h}_{kn}^{tf} \in$

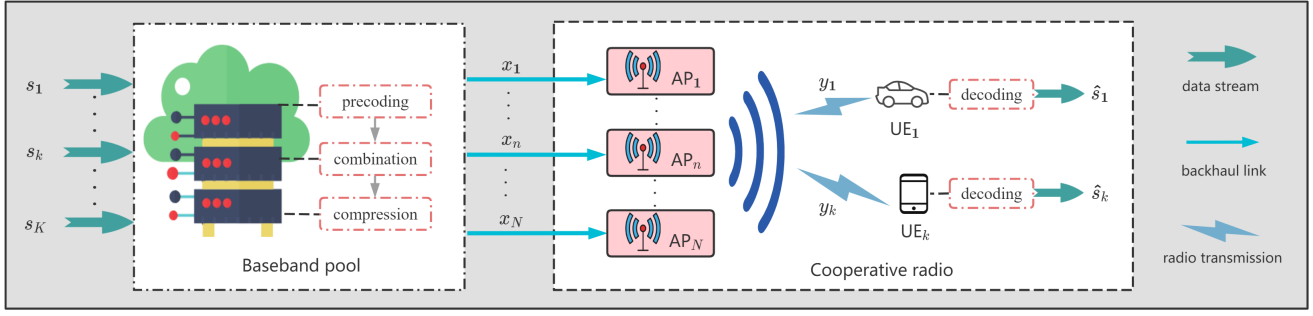


Fig. 1: System Model of an MU-MIMO Cell-free System.

$\mathbb{C}^{M \times 1}, \forall \{k, n, t, f\} \in \{\mathcal{K}, \mathcal{N}, \mathcal{T}, \mathcal{F}\}$. In the sequel, the received signal of UE_k from APs in time slot t and subcarrier f is denoted as

$$\begin{aligned}
 y_k^{tf} &= (\mathbf{h}_k^{tf})^H \sum_{k=1}^K \mathbf{w}_k^{tf} s_k^{tf} + n_k^{tf} \\
 &= \underbrace{(\mathbf{h}_k^{tf})^H \mathbf{w}_k^{tf} s_k^{tf}}_{\text{desired signal}} + \underbrace{(\mathbf{h}_k^{tf})^H \sum_{j \neq k} \mathbf{w}_j^{tf} s_j^{tf}}_{\text{interference}} \\
 &\quad + \underbrace{(\mathbf{h}_k^{tf})^H \mathbf{e}^{tf}}_{\text{quantization noise}} + \underbrace{n_k^{tf}}_{\text{background noise}}, \quad (4)
 \end{aligned}$$

where, n_k^{tf} is the complex additive white Gaussian noise with variance $(\sigma_k^{tf})^2$. Except for the background noise, an additional quantization noise is received in each user due to the operation of signal compression in AP. The signal-to-interference and noise ratio (SINR) in time slot t and subcarrier f is given by

$$\begin{aligned}
 \gamma_k^{tf}(\mathbf{w}^{tf}) &= \frac{|(\mathbf{h}_k^{tf})^H \mathbf{w}_k^{tf}|^2}{\sum_{j \neq k} |(\mathbf{h}_k^{tf})^H \mathbf{w}_j^{tf}|^2 + \sum_{n \in \mathcal{N}} \|\mathbf{h}_{kn}^{tf} \sigma_e^{tf}\|_2^2 + (\sigma_k^{tf})^2}, \quad (5)
 \end{aligned}$$

where \mathbf{w}^{tf} is the collection of $\{\mathbf{w}_k^{tf}\}, \forall k \in \mathcal{K}, \forall t \in \mathcal{T}, \forall f \in \mathcal{F}$. And the interferences from other users are treated as noise.

C. Weighted Throughput in Infinite Blocklength Regime

Based on the SINR in (5) and the Shannon capacity theory, we obtain the capacity of UE_k in INFBL regime and the WTP of the whole system as follows.

$$F_k(\mathbf{w}) = \sum_{f=1}^F \sum_{t=1}^T \log_2(1 + \gamma_k^{tf}(\mathbf{w}^{tf})), \quad (6)$$

$$C(\mathbf{w}) = \sum_{k=1}^K \rho_k F_k(\mathbf{w}), \quad (7)$$

where $\mathbf{w} = [\mathbf{w}_1^H, \dots, \mathbf{w}_K^H]^H$ is the collection of $\{\mathbf{w}_k\}$, and $\mathbf{w}_k = [\mathbf{w}_k^{11}, \dots, \mathbf{w}_k^{TF}]^H$ is the collection of $\{\mathbf{w}_k^{tf}\}, \forall \{k, t, f\} \in \{\mathcal{K}, \mathcal{T}, \mathcal{F}\}$. The weighting factor is denoted as ρ_k .

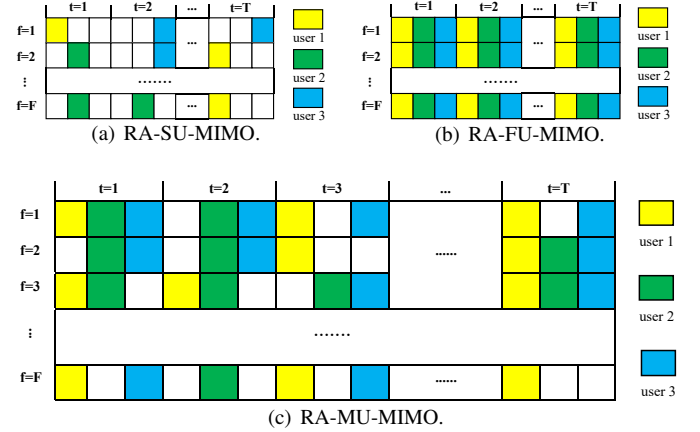


Fig. 2: Different user scheduling schemes in MU-MIMO cell-free systems (a) RA-SU-MIMO: resource allocation in single-user scheduling MIMO scenario; (b) RA-FU-MIMO: resource allocation in full-user scheduling MIMO scenario; (c) RA-MU-MIMO: resource allocation in multi-user scheduling MIMO scenario

D. Weighted Throughput in Finite Blocklength Regime

Different from the INFBL regime, the total number of bits transmitted to UE_k in a short packet is denoted as [36]

$$\Phi_k(\mathbf{w}) = \sum_{f \in \mathcal{F}} \sum_{t \in \mathcal{T}} \log_2(1 + \gamma_k^{tf}) - Q^{-1}(\epsilon) \sqrt{\sum_{f \in \mathcal{F}} \sum_{t \in \mathcal{T}} V_k^{tf}}, \quad (8)$$

where $V_k^{tf} = 1 - \frac{1}{(1 + \gamma_k^{tf})^2}$ is the channel dispersion in time slot t and subcarrier f , and the $Q^{-1}(\cdot)$ represents the inversion of Gaussian Q function with bit error probability ϵ . Ultimately, we obtain the WTP of the whole system as follow.

$$\begin{aligned}
 U(\mathbf{w}) &= \sum_{k \in \mathcal{K}} \rho_k \Phi_k(\mathbf{w}) \\
 &= \sum_{k \in \mathcal{K}} \rho_k \left(F_k(\mathbf{w}) - G_k(\mathbf{w}) \right), \quad (9)
 \end{aligned}$$

where $F_k(\mathbf{w})$ is the system capacity in INFBL regime, $G_k(\mathbf{w})$ is expressed as the following equation.

$$G_k(\mathbf{w}) = Q^{-1}(\epsilon) \sqrt{\sum_{f \in \mathcal{F}} \sum_{t \in \mathcal{T}} V_k^{tf}}. \quad (10)$$

III. SOLUTION IN INFINITE BLOCKLENGTH REGIME

In this section, we first formulate the optimization problem for maximizing the WTP of the system in INFBLL regime. User scheduling algorithm and beamformer optimization algorithm are proposed to address the WTP maximization problem.

A. Problem Formulation

According to the aforementioned analysis in Section II-C and Fig. 2, we formulate the following maximization problem of the WTP in INFBLL regime.

$$\max_{\mathbf{w}} C(\mathbf{w}) \quad (11a)$$

$$\text{s.t. } F_k(\mathbf{w}) \geq b_k, \forall k \in \mathcal{K}, \quad (11b)$$

$$\sum_{k \in \mathcal{K}} \sum_{f \in \mathcal{F}} \|\mathbf{w}_k^{tf}\|_2^2 \leq p_t, \forall f \in \mathcal{F}, \forall t \in \mathcal{T}. \quad (11c)$$

In (11), constraint (11b) ensures that the minimum number of bits for UE_k is b_k . Constraint (11c) represents that the total transmitted power on all subcarriers during the t -th transmission time slot should be no more than the maximum transmission power of the system.

We further introduce a binary variable $\zeta_k^{tf} \in \{0, 1\}, \forall \{k, t, f\} \in \{\mathcal{K}, \mathcal{T}, \mathcal{F}\}$ to represent which user is scheduled in each RE. Namely, ζ_k^{tf} equals 1 means that UE_k is scheduled in RE $\{t, f\}$, but not vice versa. Therefore, the expression of SINR in equation (5) can be rewritten as

$$\gamma_k^{tf}(\mathbf{w}^{tf}, \zeta^{tf}) = \frac{|(\mathbf{h}_k^{tf})^H \zeta_k^{tf} \mathbf{w}_k^{tf}|^2}{\sum_{j \neq k} |(\mathbf{h}_k^{tf})^H \zeta_j^{tf} \mathbf{w}_j^{tf}|^2 + \sum_{n \in \mathcal{N}} \|\mathbf{h}_{kn}^{tf} \sigma_e^{tf}\|_2^2 + (\sigma_k^{tf})^2}, \quad (12)$$

where $\zeta^{tf} = [\zeta_1^{tf}, \dots, \zeta_K^{tf}]$.

In the sequel, we transform problem (11) into problem (13)

$$\max_{\mathbf{w}, \zeta} C(\mathbf{w}, \zeta) \quad (13a)$$

$$\text{s.t. } F_k(\mathbf{w}, \zeta) \geq b_k, \quad (13b)$$

$$\sum_{k \in \mathcal{K}} \sum_{f \in \mathcal{F}} \|\zeta_k^{tf} \mathbf{w}_k^{tf}\|_2^2 \leq p_t, \quad (13c)$$

$$\zeta_k^{tf} \in \{0, 1\}, \forall k \in \mathcal{K}, \forall t \in \mathcal{T}, \forall f \in \mathcal{F}, \quad (13d)$$

where ζ is the collection of $\{\zeta_k\}$, and $\zeta_k = [\zeta_k^{11}, \dots, \zeta_k^{TF}]$, $\forall k \in \mathcal{K}$.

The objective function of problem (13) is non-convex. And it is a mixed integer nonlinear programming problem [37] due to the binary variable ζ (13d) and the non-convex constraint (13b), which is hard to be tackled. To solve this NP-hard problem, we utilize the alternating iterative optimization algorithm. In each iteration, the user scheduling algorithm based on the gene-aided (GA) algorithm [38] is first proposed to optimize the binary variable ζ with fixed beamforming vector \mathbf{w} obtained from the last iteration. Afterward, a beamforming optimization algorithm is proposed to further optimize the system performance with the fixed user scheduling scheme obtained before. Alternating iterative optimization stops until the algorithm converges.

B. User Scheduling

In this subsection, the user scheduling scheme based on the gene-aided algorithm is used to solve the binary integer programming (BIP) problem. Fig. 3 describes the process of user scheduling from the selection of variable ζ . The detailed explanations are listed as follows.

- **Initialize individual:** since the variable ζ is a binary variable which satisfies the coding space of genetic algorithm, we generate individual with binomial distribution and map the individual to ζ directly. Namely, $\zeta_{(g)} = [\zeta_{(g)}^1, \dots, \zeta_{(g)}^{Pop}]$ at the g -th generation.
- **Optimize:** after generating the individual, i.e., the time-frequency resource ζ is fixed, we next calculate the fitness of each individual x . Namely, calculate the WTP $U_{(g)}^x(\zeta_{(g)}^x)$ according to the individual and the beamforming design result (Algorithm 2 and 3).
- **Sort descending:** sort the fitnesses in descending order. Hence, the first few fitnesses have the largest values $[U_{(g)}^1, \dots, U_{(g)}^e]$.
- **Save elite:** select and keep the first e individuals $[\tilde{\zeta}_{(g)}^1, \dots, \tilde{\zeta}_{(g)}^e]$ to the next generation.
- **Crossover and mutation:** 1). the crossover probability $p_{c(g)}$ is generated randomly, if $p_{c(g)} \geq p_c$, crossover happens between individuals, e.g., $\zeta_{(g)}^x \Leftrightarrow \zeta_{(g)}^y$ means that the randomly selected row of $\zeta_{(g)}^x$ (the blue row) and the corresponding green row of $\zeta_{(g)}^y$ are exchanged between individuals x and y . 2). the mutation probability $p_{m(g)}$ is generated randomly, if $p_{m(g)} \geq p_m$, mutation occurs in each individual itself, e.g., the red element of $\zeta_{(g)}^y$ changes.
- **Generate new individual:** crossover and mutation individuals are involved in the next round of genetic selection as the new population.

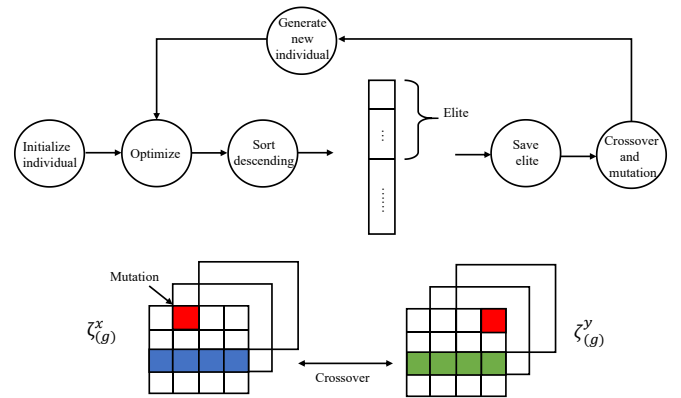


Fig. 3: Process of genetic selection.

Algorithm 1 summarizes the process of iterative optimization with user scheduling and beamforming design.

C. Beamforming Design in Infinite Blocklength Regime

With fixed user scheduling scheme, we aim to maximize the WTP of the system by beamforming design. To simplify

Algorithm 1 Joint user scheduling and beamforming design algorithm (USBDA)

- 1: **Input:** population size P_{op} , elite number e , rate r , crossover probability p_c , mutation probability p_m , maximum generation algebra g_{max} .
 - 2: **Initialize:** $g = 0$, population set $\zeta_{(g)} = [\zeta_{(g)}^1, \dots, \zeta_{(g)}^{P_{op}}]$.
 - 3: **while** $g < g_{max}$
 - 1) Calculate fitness $U_{(g)}^x$ of each individual x according to beamforming design algorithm (i.e., MMSE beamformer/Algorithm 2/Algorithm 3).
 - 2) Sort fitness $[U_{(g)}^1, \dots, U_{(g)}^{P_{op}}]$ in descending order.
 - 3) Select the first e individuals $[\tilde{\zeta}_{(g)}^1, \dots, \tilde{\zeta}_{(g)}^e]$ as the elites are reserved for the next generation.
 - 4) **if** $p_{c(g)} \geq p_c$ (crossover)
 - a) calculate the weight of the fitnesses
 - b) exchange the corresponding row between individuals.
 - 5) **end if**
 - 6) **if** $p_{m(g)} \geq p_m$ (mutation)
 - a) randomly select row number
 - b) mutation goes in the direction of the largest weight.
 - 7) **end if**
 - 8) obtain the new population.
 - 9) **if** achieve the maximum generation number g_{max}
 - a) **break**
 - 10) **end if**
 - 4: **end for**
 - 5: **Output:** ζ
-

the notation, we denote $\chi_k^{tf} = \zeta_k^{tf} \mathbf{w}_k^{tf}$. Therefore, we obtain the beamforming design problem as the following equation.

$$\max_{\chi} C(\chi) \quad (14a)$$

$$\text{s.t. } F_k(\chi) \geq b_k, \forall k \in \mathcal{K}, \quad (14b)$$

$$\sum_{k \in \mathcal{K}} \sum_{f \in \mathcal{F}} \|\chi_k^{tf}\|_2^2 \leq p_t, \forall t \in \mathcal{T}, \quad (14c)$$

where χ is the collection of $\{\chi_k^{tf}\}, \forall k \in \mathcal{K}, \forall t \in \mathcal{T}, \forall f \in \mathcal{F}$, and $\chi_k^{tf} \in \mathbb{C}^{M \times 1}$.

It is still challenging to solve problem (14) due to the non-convex objective function and constraint (14b). To solve this problem, we first denote $\mathbf{X}_k^{tf} = \chi_k^{tf} (\chi_k^{tf})^H$, $\mathbf{H}_k^{tf} = \mathbf{h}_k^{tf} (\mathbf{h}_k^{tf})^H$. Hence, SINR (12) and throughput (6) of UE_k are transformed into the following equations.

$$\gamma_k^{tf}(\mathbf{X}) = \frac{\text{Tr}(\mathbf{H}_k^{tf} \mathbf{X}_k^{tf})}{\sum_{j \neq k} \text{Tr}(\mathbf{H}_k^{tf} \mathbf{X}_j^{tf}) + (\sigma_{ke}^{tf})^2}, \quad (15)$$

$$F_k(\mathbf{X}) = \sum_{t \in \mathcal{T}} \sum_{f \in \mathcal{F}} \log_2(1 + \gamma_k^{tf}(\mathbf{X})), \quad (16)$$

where $(\sigma_{ke}^{tf})^2 = (\sigma_e^{tf})^2 \text{Tr}(\mathbf{H}_k^{tf}) + (\sigma_k^{tf})^2$ is the summation of quantization noise and background noise at UE_k in time slot t and subcarrier f . \mathbf{X} is the collection of $\mathbf{X}_k^{tf}, \forall k \in \mathcal{K}, \forall t \in \mathcal{T}$

$\mathcal{T}, \forall f \in \mathcal{F}$.

For clarity, we define the following expressions.

$$\Upsilon(\mathbf{X}) \triangleq \log_2(1 + \gamma_k^{tf}(\mathbf{X})). \quad (17)$$

$$\Upsilon_1(\mathbf{X}) \triangleq \sum_{k \in \mathcal{K}} \text{Tr}(\mathbf{H}_k^{tf} \mathbf{X}_k^{tf}) + (\sigma_k^{tf})^2. \quad (18)$$

$$\Upsilon_2(\mathbf{X}) \triangleq \sum_{j \neq k} \text{Tr}(\mathbf{H}_k^{tf} \mathbf{X}_j^{tf}) + (\sigma_k^{tf})^2. \quad (19)$$

Through some mathematical transformations after substituting (15) into (17), we can rewrite equation (17) and (16) as

$$\Upsilon(\mathbf{X}) = \log_2(\Upsilon_1(\mathbf{X})) - \log_2(\Upsilon_2(\mathbf{X})). \quad (20)$$

Equation (20) is still a non-convex function. Nevertheless, it has the form of difference of convex (DC), which can be approximated to a convex one by first order Taylor approximation. To this end, we first calculate the first derivative of (19) with respect to \mathbf{X}_j^{tf} as follow.

$$\frac{\partial \Upsilon_2(\mathbf{X})}{\partial \mathbf{X}_j^{tf}} = \frac{\mathbf{H}_k^{tf}}{\Upsilon_2(\mathbf{X}) \ln(2)}. \quad (21)$$

Therefore, equation (20) is transformed into the convex one as shown in equation (22).

$$\begin{aligned} & \bar{\Upsilon}(\mathbf{X}) \\ &= \log_2(\Upsilon_1(\mathbf{X})) - \sum_{j \neq k} \left\langle \frac{\partial \Upsilon_2(\mathbf{X})}{\partial \hat{\mathbf{X}}_j^{tf}}, (\mathbf{X}_j^{tf} - \hat{\mathbf{X}}_j^{tf}) \right\rangle \\ &= \log_2(\Upsilon_1(\mathbf{X})) - \sum_{j \neq k} \text{Tr} \left(\frac{\partial \Upsilon_2(\mathbf{X})}{\partial \hat{\mathbf{X}}_j^{tf}} (\mathbf{X}_j^{tf} - \hat{\mathbf{X}}_j^{tf})^H \right). \end{aligned} \quad (22)$$

where $\hat{\mathbf{X}}_j^{tf}$ is obtained from the last iteration result.

For notation simplicity, we define $\bar{F}_k(\mathbf{X}) \triangleq \sum_{t \in \mathcal{T}} \sum_{f \in \mathcal{F}} \bar{\Upsilon}(\mathbf{X})$. In the sequel, the equivalence of problem (14) is denoted as

$$\max_{\mathbf{X}} \sum_{k \in \mathcal{K}} \bar{F}_k(\mathbf{X}) \quad (23a)$$

$$\text{s.t. } \bar{F}_k(\mathbf{X}) \geq b_k, \quad (23b)$$

$$\sum_{k \in \mathcal{K}} \sum_{f \in \mathcal{F}} \text{Tr}(\mathbf{X}_k^{tf}) \leq p_t, \quad (23c)$$

$$\text{Rank}(\mathbf{X}_k^{tf}) \leq 1, \quad (23d)$$

$$\mathbf{X}_k^{tf} \succeq 0, \forall k \in \mathcal{K}, \forall t \in \mathcal{T}, \forall f \in \mathcal{F}, \quad (23e)$$

where $\text{Rank}(\cdot)$ represents the rank of a matrix and \succeq stands for the semi-positive definite.

Since the constraint (23d) is non-convex, we first drop it by utilizing the semidefinite relaxation (SDR) method, thus problem (23) is transformed into problem (24).

$$\max_{\mathbf{X}} \sum_{k \in \mathcal{K}} \bar{F}_k(\mathbf{X}) \quad (24a)$$

$$\text{s.t. } (23b), (23c), (23e). \quad (24b)$$

It is not difficult to see that problem (24) is convex relative to variable \mathbf{X} , which can be solved by some standard optimization tools (e.g., CVX). Furthermore, the eigendecomposition method or Gaussian randomization method is adopted to

recover the BF vector $\boldsymbol{\chi}$ from \mathbf{X} .

Algorithm 2 concludes the beamforming design based on the SDR method in INFBL regime.

Algorithm 2 Beamforming design algorithm in INFBL regime (BF-INFBL)

- 1: **Input:** the channel gain $\mathbf{h}_k^{tf}, \forall k, \in \mathcal{K}, \forall t \in \mathcal{T}, \forall f \in \mathcal{F}$, maximum iteration number is i_{\max} .
 - 2: **Initialize:** the beamforming vector $(\boldsymbol{\chi}_t^{tf})^{(0)}$ is initialized by MMSE beamformer. Calculate $(\mathbf{X}_k^{tf})^{(0)} = (\boldsymbol{\chi}_t^{tf})^{(0)}((\boldsymbol{\chi}_t^{tf})^{(0)})^H, \mathbf{H}_k^{tf} = \mathbf{h}_k^{tf}(\mathbf{h}_k^{tf})^H$.
 - 3: **for** each iteration i
 - 1) Calculate $\gamma_k^{tf}((\mathbf{X})^{(i)})$ according to equation (15).
 - 2) Calculate $\bar{\mathbf{Y}}((\mathbf{X})^{(i)})$ according to (22).
 - 3) Solve problem (24) to obtain $(\mathbf{X})^{(i)}$.
 - 4) Calculate the WTP according to the objective function of (24).
 - 5) Update the iteration number: $i = i + 1$.
 - a) $(\mathbf{X}_k^{tf})^{(i+1)} \leftarrow (\mathbf{X}_k^{tf})^{(i)}$.
 - b) $i \leftarrow i + 1$.
 - 6) **if** achieve the maximum iteration number i_{\max}
 - a) **break**.
 - 7) **end if**
 - 4: **end for**
 - 5: **Output:** $(\mathbf{X})^{i_{\max}}$.
 - 6: Recovery the beamforming vector $\boldsymbol{\chi}$ from \mathbf{X} by eigendecomposition method or Gaussian randomization.
 - 7: Calculate the WTP according to the objective function of problem (24).
-

IV. SOLUTION IN FINITE BLOCKLENGTH REGIME

A. Problem Formulation

In this section, we formulate and address the optimization problems for maximizing the WTP of the whole system by user scheduling and beamforming design in FBL regime. As shown in Fig. 2, the colored patch indicates that the corresponding user is scheduled while the blank patch indicates no service. Hence, the latency in FBL regime is equal to or greater than the blocklength.

Based on Fig. 2, we formulate the following optimization problem to maximize the WTP of the whole system in FBL regime.

$$\max_{\mathbf{w}} U(\mathbf{w}) \quad (25a)$$

$$\text{s.t. } F_k(\mathbf{w}) - G_k(\mathbf{w}) \geq b_k, \forall k \in \mathcal{K}, \quad (25b)$$

$$\sum_{k \in \mathcal{K}} \sum_{f \in \mathcal{F}} \|\mathbf{w}_k^{tf}\|_2^2 \leq p_t, \forall t \in \mathcal{T}, \forall f \in \mathcal{F}. \quad (25c)$$

In (25), constraint (25b) represents the minimum transmit data requirement to satisfy the QoS of each user. Constraint (25c) means that the total transmission power on the total subcarriers at t -th transmission duration should be less than the total transmission power. Similar to the user scheduling scheme in INFBL regime, we rewrite problem (25) into the

following equivalent problem by introducing a binary variable ζ .

$$\max_{\mathbf{w}, \zeta} U(\mathbf{w}, \zeta) \quad (26a)$$

$$\text{s.t. } F_k(\mathbf{w}, \zeta) - G_k(\mathbf{w}, \zeta) \geq b_k, \quad (26b)$$

$$\sum_{k \in \mathcal{K}} \sum_{f \in \mathcal{F}} \|\zeta_k^{tf} \mathbf{w}_k^{tf}\|_2^2 \leq p_t, \quad (26c)$$

$$\zeta_k^{tf} \in \{0, 1\}, \forall k \in \mathcal{K}, \forall t \in \mathcal{T}, \forall f \in \mathcal{F}. \quad (26d)$$

Remark 1. Similarly, ζ_k^{tf} denotes whether UE_k is scheduled in resource element $\{t, f\}$. In addition, we point out that the summation of time slots in each subcarrier represents the maximum latency requirement in FBL regime. And the relationship between the blocklength L_k^f of UE_k in subcarrier f and the indicator factor ζ_k^f is formulated as the ℓ_0 -norm of ζ_k^f , i.e.,

$$L_k^f = \|\zeta_k^f\|_0, \forall k \in \mathcal{K}, \forall f \in \mathcal{F}. \quad (27)$$

Furthermore, the transmission latency is greater than or equal to the blocklength but not more than the maximum transmission latency T to meet the latency requirement for URLLC transmission.

B. Beamforming Design in Finite Blocklength Regime

As same as problem (13), problem (26) is an MINLP problem which is intractable to address. Hence, we decompose the problem into two subproblems, including user scheduling and beamforming design. And these two subproblems are solved in turn iteratively. Since the user scheduling algorithm has been given in Algorithm 1, here we omit it due to space limitations.

In the sequel, we aim to optimize the beamforming vector \mathbf{w}_k^{tf} with fixed ζ . As same as Section III-C, by utilizing the semidefinite relaxation method, problem (26) is transformed as

$$\max_{\mathbf{X}} U(\mathbf{X}) \quad (28a)$$

$$\text{s.t. } F_k(\mathbf{X}) - G_k(\mathbf{X}) \geq b_k, \quad (28b)$$

$$\sum_{k \in \mathcal{K}} \sum_{f \in \mathcal{F}} \text{Tr}(\mathbf{X}_k^{tf}) \leq p_t, \quad (28c)$$

$$\text{Rank}(\mathbf{X}_k^{tf}) \leq 1, \quad (28d)$$

$$\mathbf{X}_k^{tf} \geq 0, \forall k \in \mathcal{K}, \forall f \in \mathcal{F}, \forall t \in \mathcal{T}. \quad (28e)$$

For simplicity, we let

$$I_k^{tf}(\mathbf{X}) \triangleq \sum_{j \neq k} \text{Tr}(\mathbf{H}_k^f \mathbf{X}_j^{tf}). \quad (29)$$

Since the constraint (28d) is nonconvex, we first drop it. In addition, the objective function is nonconvex, and we introduce a series of auxiliary variables $\mathbf{z} = \{z_k, \forall k \in \mathcal{K}\}$, $\mathbf{z}_k = [z_k^{11}, \dots, z_k^{TF}]^T$ to bound the SINRs, hence the problem

(28) is rewritten as

$$\max_{\mathbf{X}, \mathbf{z}} U(\mathbf{z}) \quad (30a)$$

$$\text{s.t. } F_k(\mathbf{z}_k) - G_k(\mathbf{z}_k) \geq b_k, \quad (30b)$$

$$z_k^0 \leq z_k^{tf} \leq \gamma_k^{tf}, \forall k \in \mathcal{K}, \forall f \in \mathcal{F}, \forall t \in \mathcal{T}, \quad (30c)$$

$$(28c), (28e), \quad (30d)$$

where z_k^0 is the minimum SINR boundary, $U(\mathbf{z}_k)$, $F_k(\mathbf{z}_k)$, $G_k(\mathbf{z}_k)$ are denoted as

$$U(\mathbf{z}) = \sum_{k \in \mathcal{K}} \rho_k \left(F_k(\mathbf{z}_k) - G_k(\mathbf{z}_k) \right). \quad (31)$$

$$F_k(\mathbf{z}_k) = \sum_{f \in \mathcal{F}} \sum_{t \in \mathcal{T}} \log_2 \left(1 + z_k^{tf} \right). \quad (32)$$

$$G_k(\mathbf{z}_k) = Q^{-1}(\epsilon) \sqrt{V_k(\mathbf{z}_k)}. \quad (33)$$

$$V_k(\mathbf{z}_k) = \sum_{f \in \mathcal{F}} \sum_{t \in \mathcal{T}} \left(1 - (1 + z_k^{tf})^{-2} \right). \quad (34)$$

Since the objective function in (31) has the form of difference of convex, we can approximate $G_k(\mathbf{z}_k)$ by first order Taylor expansion.

$$\begin{aligned} G_k(\mathbf{z}_k) &\leq \bar{G}_k(\mathbf{z}_k) \\ &= G_k(\mathbf{z}_k^{(iter)}) + \nabla_{\mathbf{z}_k} G_k(\mathbf{z}_k)^T \left(\mathbf{z}_k - \mathbf{z}_k^{(iter)} \right), \end{aligned} \quad (35)$$

where,

$$\nabla_{\mathbf{z}_k} G_k(\mathbf{z}_k) = \frac{1}{\sqrt{V_k(\mathbf{z}_k^{(iter)})}} \begin{bmatrix} (1 + z_k^1)^{-3} \\ (1 + z_k^2)^{-3} \\ \vdots \\ (1 + z_k^T)^{-3} \end{bmatrix}. \quad (36)$$

To step further, the auxiliary variables $\pi_k^{tf}, \theta_k^{tf}, \forall k, t, f$ are introduced to approximate the SINRs, hence the constraint (30c) can be expressed as the following inequality,

$$z_k^0 \leq z_k^{tf} \leq \frac{(\pi_k^{tf})^2}{\theta_k^{tf}} \leq \gamma_k^{tf}, \quad (37)$$

where

$$(\pi_k^{tf})^2 \leq d_k^{tf} \text{Tr} \left(\mathbf{H}_k^f \mathbf{X}_k^{tf} \right). \quad (38)$$

$$\theta_k^{tf} \geq I_k^{tf} + (\sigma_{ke}^{tf})^2. \quad (39)$$

Since the constraints (37) and (38) are still nonconvex, we further approximate them into the convex one by applying first order Taylor expression which are denoted as the following expressions.

$$(\pi_k^{tf})^2 \geq 2\hat{\pi}_k^{tf} \pi_k^{tf} - (\hat{\pi}_k^{tf})^2. \quad (40)$$

$$\frac{(\pi_k^{tf})^2}{\theta_k^{tf}} \geq \frac{2\hat{\pi}_k^{tf}}{\hat{\theta}_k^{tf}} \pi_k^{tf} - \left(\frac{\hat{\pi}_k^{tf}}{\hat{\theta}_k^{tf}} \right)^2 \theta_k^{tf}. \quad (41)$$

In the end, we obtain the following approximation problem (42), which is a convex problem and can be solved by standard optimization tools. The process of beamforming design is

summarized in Algorithm 3.

$$\max_{\mathbf{X}, \mathbf{z}, \boldsymbol{\pi}, \boldsymbol{\theta}} \sum_{k=1}^K \rho_k \left(F_k(\mathbf{z}_k) - \bar{G}_k(\mathbf{z}_k) \right) \quad (42a)$$

$$\text{s.t. } (30b), (30d), (39) \sim (41), \quad (42b)$$

where $\boldsymbol{\pi} = \{\pi_k^{tf}, \forall k \in \mathcal{K}, \forall f \in \mathcal{F}, \forall t \in \mathcal{T}\}$, $\boldsymbol{\theta} = \{\theta_k^{tf}, \forall k \in \mathcal{K}, \forall f \in \mathcal{F}, \forall t \in \mathcal{T}\}$.

Algorithm 3 Beamforming design in FBL regime (BF-FBL)

- 1: **Input:** the channel gain $\mathbf{h}_k^{tf}, \forall k \in \mathcal{K}, \forall f \in \mathcal{F}, \forall t \in \mathcal{T}$, maximum iteration number is i_{\max} .
 - 2: **Initialize:** the beamforming vector $(\boldsymbol{\chi}_k^{tf})^0$ is initialized by MMSE beamformer. In the sequel, $(\mathbf{X}_k^{tf})^{(0)}, (z_k^{tf})^{(0)}, (\pi_k^{tf})^{(0)}$ and $(\theta_k^{tf})^{(0)}$ are obtained.
 - 3: **for** each iteration i
 - 1) Solve problem (42) using CVX tool with SDP solver, and obtain the variables of $(\mathbf{X}_k^{tf})^{(i)}, (z_k^{tf})^{(i)}, (\pi_k^{tf})^{(i)}, (\theta_k^{tf})^{(i)}$.
 - 2) Calculate the WTP $U(\mathbf{X})$.
 - 3) Update the following variables
 - a) $(\mathbf{X}_k^{tf})^{(i+1)} \leftarrow (\mathbf{X}_k^{tf})^{(i)}$.
 - b) $(z_k^{tf})^{(i+1)} \leftarrow (z_k^{tf})^{(i)}$.
 - c) $(\pi_k^{tf})^{(i+1)} \leftarrow (\pi_k^{tf})^{(i)}$.
 - d) $(\theta_k^{tf})^{(i+1)} \leftarrow (\theta_k^{tf})^{(i)}$.
 - e) $i = i + 1$.
 - 4) **if** achieve the maximum iteration number i_{\max}
 - a) **break**.
 - 5) **end if**
 - 4: **end for**
 - 5: **Output:** $(\mathbf{X}_k^{tf})^{(i)}, (z_k^{tf})^{(i)}, (\pi_k^{tf})^{(i)}, (\theta_k^{tf})^{(i)}$.
 - 6: Recovery the beamforming vector $\boldsymbol{\chi}_k^{tf}$ from \mathbf{X}_k^{tf} by eigendecomposition method or Gaussian randomization.
-

C. Complexity Analysis

Since problem (24) consists of K variables, $KTF + K + T$ constraints are solved by the CVX solver within the polynomial time. Therefore, the computational complexity of Algorithm 2 is $\mathcal{O}(K^3(KTF + T + K))$ [39]. Similarly, $4K$ variables and $3KTF + T + K$ constraints in problem (42). The computational complexity of Algorithm 3 is $\mathcal{O}((4K)^3(3KTF + T + K))$. In addition, the computational complexity of the GA method grows linearly with the number of generations and the population increase. To this end, the computational complexity of Algorithm 1 with Algorithm 2 and Algorithm 3 equal to $\mathcal{O}((Pop)e)K^3(KTF + T + K)$ and $\mathcal{O}((Pop)e)(4K)^3(3KTF + T + K)$.

D. Cell-free System vs Centralized Antenna System

Actually, our proposed user scheduling method can be easily extended to the centralized antenna system (CAS). The transmitting signal in each TF resource from centralized base station (BS) is expressed as

$$\hat{\mathbf{x}}^{tf} = \sum_{k \in \mathcal{K}} \hat{\mathbf{w}}_k^{tf} s_k^{tf} + \mathbf{e}_{\text{BS}}^{tf}. \quad (43)$$

where $\hat{\mathbf{w}}_k^{tf} \in \mathbb{C}^{M_c \times 1}, \forall k \in \mathcal{K}$ is the beamforming vector. M_c and e_{BS}^{tf} are number of antennas of BS and the quantization noise at BS.

In the sequel, we obtain the received signal and the SINR of DV_k denoted as

$$\hat{y}_k^{tf} = (\mathbf{h}_k^{tf})^H \sum_{k \in \mathcal{K}} \hat{\mathbf{w}}_k^{tf} s_j^{tf} + (\mathbf{h}_k^{tf})^H e_{\text{BS}}^{tf} + n_k^{tf}, \quad (44)$$

$$\hat{\gamma}_k^{tf} = \frac{|(\mathbf{h}_k^{tf})^H \hat{\mathbf{w}}_k^{tf}|^2}{\sum_{j \neq k} |(\mathbf{h}_k^{tf})^H \hat{\mathbf{w}}_j^{tf}|^2 + |(\mathbf{h}_k^{tf})^H \sigma_{\text{BS}}^2|^2 + (\sigma_k^{tf})^2}. \quad (45)$$

The WTP of CAS in FBL and INFBL regimes is the same as that of CF systems. Comparing (43)~(45) and (1)~(5), we find that the distributed antenna cooperation that in CF systems disappears in CAS. Unlike the CF systems, CAS is incapable of distributed antenna collaboration due to the centralized antenna deployment. Therefore, it is beneficial to operate user scheduling in different TF resource to achieve diversity gains. As we know, only considering path loss, the theoretical channel capacity difference between CF systems and CAS can be denoted as the following expression related to the user position [40].

$$\Delta(\mathbf{d}) = \log_2 \left[\sum_{n=1}^N \left(\frac{D}{d_n} \right)^{\eta_0} \right] - \log_2 \left[\left(\frac{D}{d_0} \right)^{\eta_0} \right] \quad (46)$$

where d_n stands for the distance between DV and AP_n. $\mathbf{d} = [d_1, \dots, d_N]$, d_0 is the distance between DV and the centralized BS. D, η_0 represent the reference distance and fading exponent.

Remark 2. *It is seen that the system performance of CF systems and CAS is related to the position of users shown in (46). Although the performance of the CF system may be worse than CAS (i.e., users are distributed near the center of the system), its capacity coverage is more uniform and easier to achieve better system performance since the distributed antennas more closer to users, especially when users are dispersed throughout the entire system.*

Simulation results give the numerical comparison of CAS and CF systems in our proposed scenario.

V. NUMERICAL RESULTS

In this section, we present numerical results to demonstrate our resource allocation algorithm in CF systems with INFBL regime and FBL regime. And the system performance between CAS and CF systems is analyzed. Besides, we compare the resource allocation scheme in MU-MIMO, FU-MIMO and SU-MIMO scenarios. Simulation parameters are given in TABLE I. In cell-free MU-MIMO MC systems, APs and UEs are distributed within 500m radius randomly. The channel coefficients $\{\mathbf{h}_k^{tf}\}, \forall k \in \mathcal{K}, \forall t \in \mathcal{T}, \forall f \in \mathcal{F}$ are modeled as $\mathbf{h}_k^{tf} = \eta_k^{tf} \bar{\mathbf{h}}_k^{tf}$, where $\bar{\mathbf{h}}_k^{tf}$ is independent and identically distribution (iid) $\sim \mathcal{CN}(0, 1)$. The channel gain η_k^{tf} equals $\frac{1}{1+(d_{kn}/D)^{\eta_0}}$, where d_{kn} represent the distance between AP_n and UE_k, respectively. We denote $N = 8, M = 2, K = 16, \epsilon = 10^{-5}, F = 3, T = 6$, unless otherwise specified.

TABLE I: Simulation Parameters

parameter	value
cell radius (r)	500m
crossover probability (p_c)	0.8
mutation probability (p_m)	0.9
signal to noise (SNR)	40dB
decoding error probability (ϵ)	$10^{-1} \sim 10^{-9}$
number of APs (N)	1,2,4,8,16
number of users (K)	1,2,8,16,24
number of subcarriers (F)	1~5
the maximum latency (T)	2,4,6,8,10

Fig. 4 shows the convergence of the beamforming (BF) design algorithms, including Algorithm 2 and 3 in INFBL and FBL regimes, respectively. It is seen that the WTP of each scheme converges quickly, almost within 2 iterations. Besides, with the same blocklength, the RA-MU-MIMO scheme in CF systems achieves higher performance gain than that in CAS. Similarly, with the same systems, the performance gain of the RA-MU-MIMO scheme in the INFBL regime is better than that in the FBL regime. The detailed performance gains is compared in TABLE II.

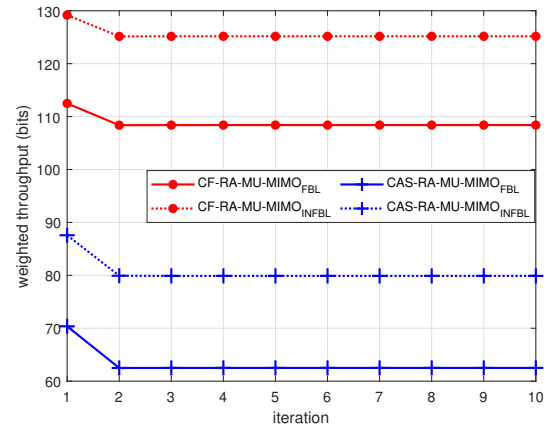


Fig. 4: Convergence of the beamforming design in CAS and CF systems with infinite and FBL.

TABLE II: Comparison of the performance gains

Scenario	Performance gain
CF system	INFBL > FBL: 13.41%
CAS sytem	INFBL > FBL: 21.81%
FBL regime	CF > CAS: 42.34%
INFBL regime	CF > CAS: 36.14%

Fig. 5 illustrates the convergence of the joint user scheduling and beamforming design algorithm (Algorithm 1). In each generation of user scheduling, the fitness of each individual is obtained from beamforming design result, where beamforming design algorithm is included in Algorithm 1. The computational complexity of the proposed beamforming method is much higher than that of the linear MMSE beamformer. Therefore, two-stage algorithm is applied to the Algorithm

1. We first replace the proposed beamforming method with linear MMSE beamformer for calculating the fitness function for each individual in the first stage. Finally, the convergent user scheduling optimization result and the optimal fitness value based on the linear MMSE beamformer are obtained as shown in Fig. 5-stage 1. In the second stage, the obtained user scheduling scheme is set as the initial value of user scheduling scheme in the next ten generations of the Algorithm 1, where the proposed beamforming method is adopted in these ten generations. As shown in Fig. 5-stage 2, the WPT remains unchanged during the total ten generations both with FBL and INFBL regimes in CAS, while that in CF systems keeps changing within 2 generations, which verifies that the MMSE beamformer instead of the proposed beamforming design method in Algorithm 1 can ultimately obtain the same user scheduling optimization result and greatly reduce the computational complexity. Namely, Algorithm 1 with proposed beamformer converges within ten generations with a better initial user scheduling scheme obtained from linear and low computational complexity MMSE beamformer pre-used.

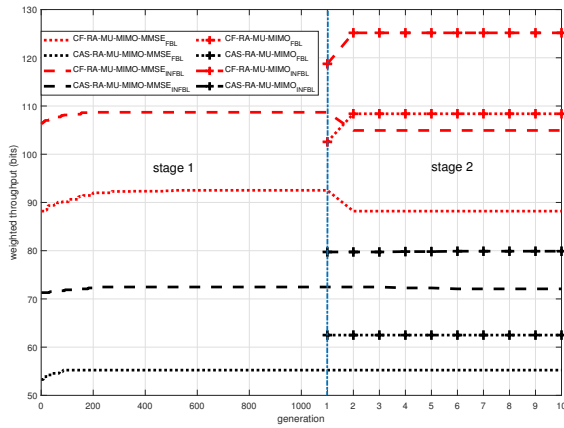


Fig. 5: Convergence of the joint user scheduling and beamforming design of Algorithm 1.

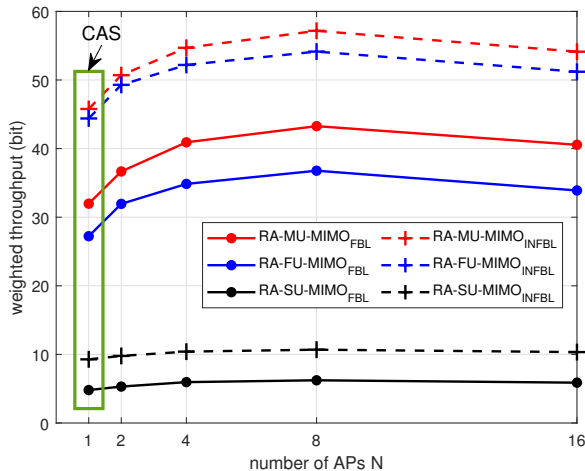


Fig. 6: Impact of the number of APs on WTP.

In Fig. 6, the WPT under different numbers of APs is given to show the impact of the spatial DoF and array gain on WPT. The total number of antennas equals 16. Hence, the number of APs equals 1 (i.e., in CAS) and 16 (i.e., in CF systems) means there are only array gain and spatial DoF, which leads to lower WPT. We find that when the number of APs equals 8, the joint effect of spatial DoF and array gain enables WPT to reach its maximum value. It is seen that the system performance in this scenario is not directly related to the number of APs. It may be related to the trade-off between array gain and spatial DoF. However, the WPT in CF systems is superior to that in CAS. And the RA-MU-MIMO scheme achieves the highest WPT than its comparison schemes both in CAS and CF systems with FBL and INFBL regimes. Similarly, the WPT of each resource allocation scheme in the INFBL regime is higher than its counterpart in the FBL regime due to INFBL and error-free assumption.

Fig. 7 studies the impact of the maximum latency on the WPT of three resource allocation methods in CAS and CF systems with FBL. The increasing maximum latency leads to more time-resource being utilized, resulting in higher WPT of all schemes. And the WPT of each scheme in CF systems is superior to its counterpart in CAS, owing to the additional spatial DoF. Under the same maximum latency, RA-MU-MIMO scheme obtains the highest WPT compared to the other two methods, while the RA-SU-MIMO scheme achieves the lowest WPT among the three resource allocation schemes. However, the performance gap between MU-MIMO and FU-MIMO is smaller than that between MU-MIMO/FU-MIMO and SU-MIMO due to the multiuser MIMO diversity gain. Nevertheless, the computational complexity of the RA-MU-MIMO scheme is likely to be reduced compared to the RA-FU-MIMO scheme since the computational complexity of BF-FBL equals $\mathcal{O}((4K)^3(3KTF + T + K))$ which is related to the number of users. In addition, the WTP of RA-SU-MIMO equals 0 when $T = \{2, 4\}$, because the number of users $K = 16$ is greater than the total resources elements $T \times F = \{6, 12\}$ that is not able to satisfy the QoS of some users in RA-SU-MIMO scheme in which one RE almost serves one user.

As shown in Fig. 8, we describe the impact of the decoding error probability (DEP) on WPT in FBL regime. For each resource allocation scheme, higher WPT is obtained with a higher DEP, but the reliability of the system is significantly reduced. In Fig. 8(a), we find that the WPT of each scheme in CF system is higher than its corresponding scheme in CAS. In Fig. 8(b), under the given DEP (i.e., the reliability requirement), higher WPT of each method can be achieved by increasing more number of time slots T (i.e., the maximum latency requirements). Therefore, the performance improvement of two of the WPT, reliability, and latency will inevitably lead to the performance degradation of the remaining one, which suggests a performance trade-off among them. However, both in Fig. 8(a) and Fig. 8(b), the performance of the RA-MU-MIMO scheme is superior to that of the counterparts. When the DEP is larger than 10^{-7} , the WPT of RA-MU-MIMO in CAS starts exceeding that of RA-FU-MIMO in CF systems. Similarly, the RA-SU-MIMO scheme has the lowest WPT

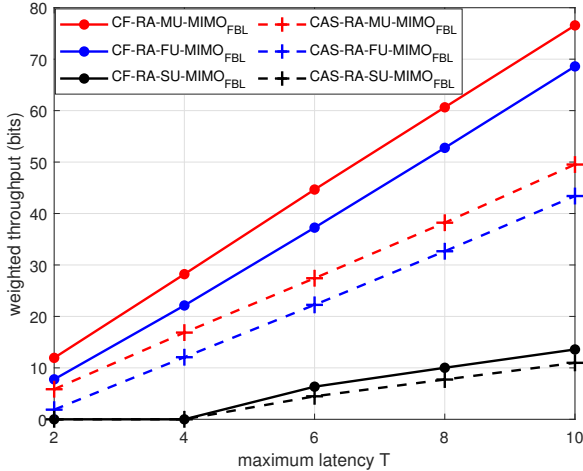
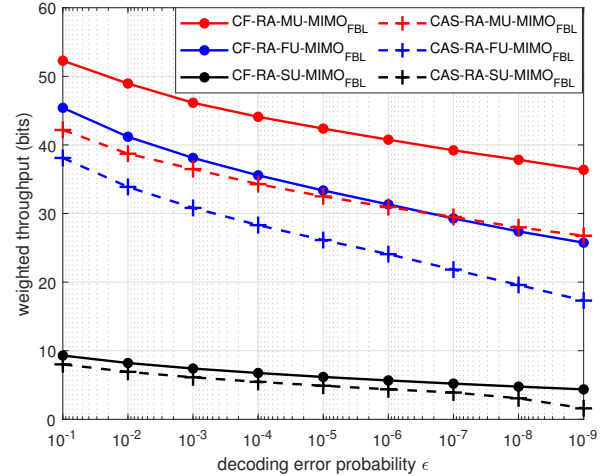


Fig. 7: Impact of the maximum latency on WTP in FBL regime.

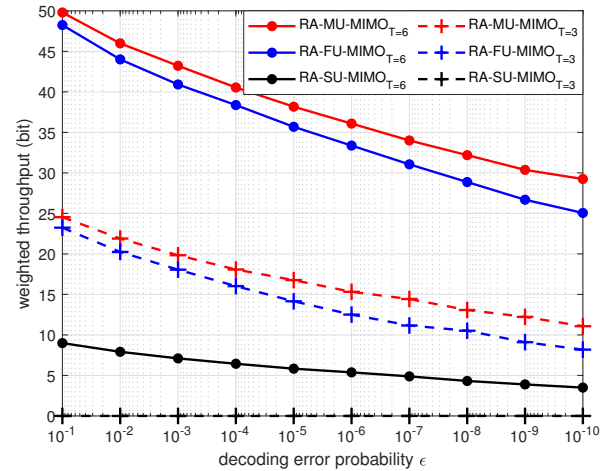
under the same DEP compared to the other two schemes. Besides, the superiority of the RA-MU-MIMO scheme appears significantly when the DEP decreases and the time resources are limited. On the one hand, the WPT gap between the RA-MU-MIMO scheme and the RA-FU-MIMO scheme gradually widens with the DEP decreases. On the other hand, the QoS of users in RA-SU-MIMO scheme is unable to be satisfied due to resource deficiency leading to the zero WPT. To this end, it is necessary to operate RA-MU-MIMO to balance the system performance and limited resources.

Fig. 9 investigates the impact of the number of subcarriers on the WPT. With the increasing of the subcarriers, the WPT of each resource allocation scheme increases as well, which benefits from the frequency diversity. Thereinto, the RA-SU-MIMO scheme acquires the lowest WPT compared to the other two resource allocation schemes both in Fig. 9(a) ~ Fig. 9(c). What's more, the WPT of RA-SU-MIMO scheme equals 0 when the number of subcarriers equal $F = \{1, 2\}$, and the corresponding total REs is $T \times F = \{6, 12\}$ which is less than the number of users. Therefore, the QoS of some users is unable to be satisfied resulting in the zero value of the WPT. However, RA-MU-MIMO and RA-FU-MIMO schemes may avoid the situation mentioned in the RA-SU-MIMO scheme due to insufficient resource usage, as multiple or all users are served on each time-frequency resource. Therefore, these two resource allocation schemes have higher resource utilization than the RA-SU-MIMO scheme. Similarly, it is seen that the WPT of each scheme in CF systems is greater than that in CAS due to spatial DoF both in FBL and INFBL regimes shown in Fig. 9(a) and Fig. 9(b).

In Fig. 10, we further explore the impact of the number of users on WPT. As the number of users increases, the WPT of all resource allocation schemes decreases, because the inter-user interference increases gradually with increasing users. Furthermore, the resources are allocated to more users with diverse channel gain which leads to system performance degradation. Besides, when the number of users equals 1



(a) CF vs CAS in FBL regime



(b) The trade-off among the WPT, latency and reliability

Fig. 8: Impact of the decoding error probability on WTP in FBL regime.

(i.e., $K=1$), three resource allocation schemes in CF systems achieve almost the same performance gain. When the number of antennas is larger than the number of users (i.e., $K < 16$), the RA-MU-MIMO and RA-FU-MIMO schemes obtain the same WPT. Meanwhile, the WPT of RA-MU-MIMO and RA-FU-MIMO schemes in CAS exceeds that in CF systems shown in Fig. 10(a) and Fig. 10(b) since the array gain may be greater than the spatial DoF in this situation. As the number of users approaches the number of antennas, the WPT of RA-MU-MIMO scheme is better than that of RA-FU-MIMO scheme both in CAS and CF systems with FBL and INFBL. And the WPT of each resource allocation scheme in CF systems is higher than its counterpart in CAS. To further increase the number of users (i.e., the number of users is greater than that of the antennas and REs), it is seen that not only the RA-SU-MIMO scheme but also the RA-FU-MIMO scheme are unable to satisfy the QoS of each user while the system performance of the RA-MU-MIMO scheme may still steadily decrease with

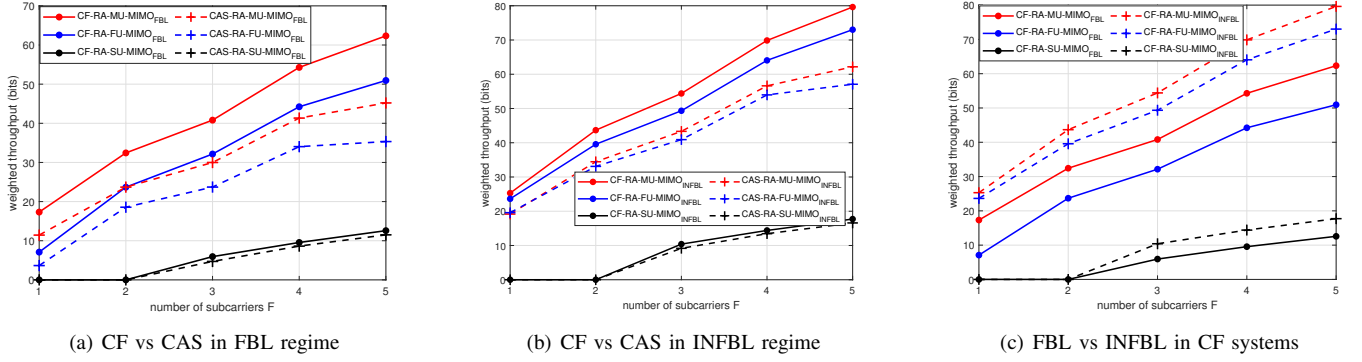


Fig. 9: Impact of the number of subcarriers on weighted throughput.

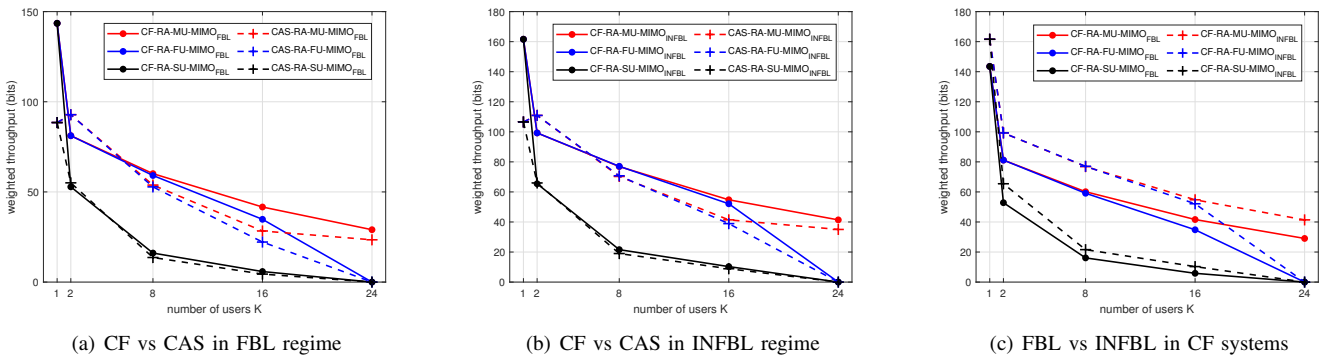


Fig. 10: Impact of the number of users on weighted throughput.

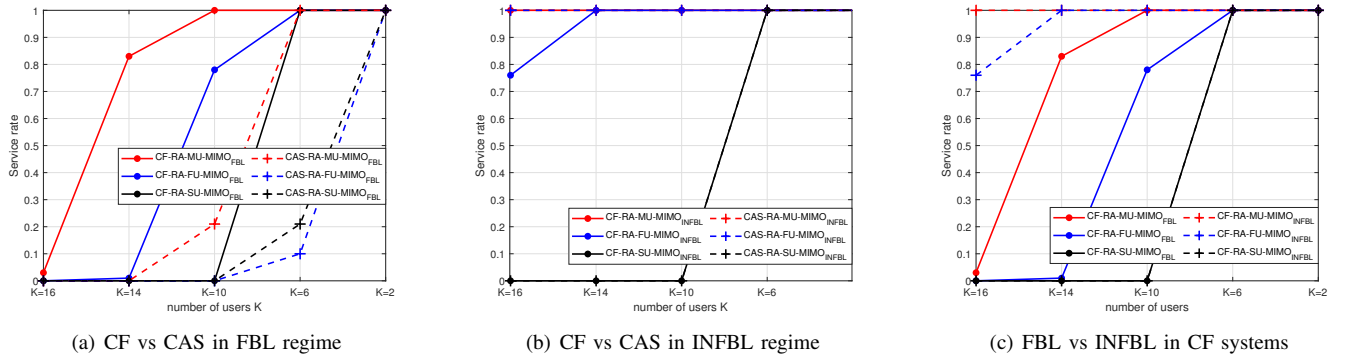


Fig. 11: Service rate of each resource allocation in CAS and CF systems with FBL and INFBL.

the increased number of users. In Fig. 11, we discuss the service rate (SR) of each resource allocation scheme under different numbers of users both in CAS and CF systems with FBL and INFBL, where SR represents the proportion of the number of Monte Carlo simulations that meet the QoS for all users to the overall number of Monte Carlo simulations. The total resource elements equals $T \times F = 6$, the number of APs in CF systems is 6 and the number of antennas per AP is 2 (i.e., the total number of antennas is 12). As shown in the figure, when the number of users exceeds the number of

resource elements, the SR of users in RA-SU-MIMO equals zero since the resource elements are not adequate for each user without inter-user interference. And the SR in the RA-FU-MIMO scheme in CAS with FBL is even lower than that of RA-SU-MIMO which may be caused by the severe inter-user interference. Furthermore, when the number of antennas is less than the number of users, the SR of users approaches zero for all of the resource allocation schemes since the spatial DoF is lacking for the increasing number of users. However, the SR of the RA-MU-MIMO scheme is greater than that of the counterparts under the same number of users, which means the importance of resource allocation. Besides, the SR of users in

the INFBL regime is superior to that in its corresponding FBL regime in Fig. 11(c) due to INFBL and error-free assumption. In addition, the SR of each resource allocation scheme in CF systems with INFBL is the same as that in CAS, while the SR of each resource allocation scheme in CF systems with FBL is better than that in CAS, which indicates that the system performance in FBL regime may be more sensitive than that in INFBL regime due to the impact of channel dispersion.

VI. CONCLUSION

In this paper, we investigated the maximization problem of WTP in a CF MU-MIMO MC system both with FBL and INFBL, where the constraints of the total system power consumption and the minimum QoS of each user are satisfied. We jointly optimized the user scheduling scheme and the beamformer to maximize the system performance in INFBL regime and FBL regime under the given BLER and the maximum latency. Since the problem is a MINLP problem which is highly non-convex, a nested iteration algorithm (USBDA) based on GA and SCA was proposed to efficiently solve this intractable issue. To step further, a two-stage algorithm was used for the USBDA algorithm to reduce the computational complexity which was verified in the Section V. Besides, simulation results verified that CF architecture provides more spatial DoF to achieve higher spectral efficiency compared to the CAS. In addition, the proposed RA-MU-MIMO resource allocation scheme is superior to the other two comparison resource allocation schemes, including RA-SU-MIMO and RA-FU-MIMO resource allocation schemes, resulting in higher WTP with limited resources certainly both in CAS and CF systems. What's more, we found that the proposed resource allocation scheme in the FBL regime is more suitable for URLLC scenarios where the latency and reliability are strictly met, while that in the INFBL regime is more satisfied for eMBB scenarios with infinite blocklength and error-free assumptions. Furthermore, more TF resources and antennas lead to higher system performance due to multiplexing gain and diversity gain. And the system performance in CF systems is superior to that of its collocated counterpart as the number of users continuously increases due to the more spatial DoF in CF systems. Nevertheless, when the number of users is quite small, the system performance in CAS is better than CF systems resulting from the array gain.

REFERENCES

- [1] X. You, "6G Extreme Connectivity via Exploring Spatiotemporal Exchangeability," *Sci China Inf Sci*, 2022, doi: doi.org/10.1007/s11432-022-3598-4.
- [2] M. Alonzo, P. Baracca, S. R. Khosravirad and S. Buzzi, "Cell-Free and User-Centric Massive MIMO Architectures for Reliable Communications in Indoor Factory Environments," *IEEE Open Journal of the Communications Society*, vol. 2, pp. 1390-1404, 2021, doi: 10.1109/OJ-COMS.2021.3089281.
- [3] F. Boabang, A. Ebrahimzadeh, R. H. Glitho, H. Elbiaze, M. Maier and F. Belqasmi, "A Machine Learning Framework for Handling Delayed/Lost Packets in Tactile Internet Remote Robotic Surgery," *IEEE Transactions on Network and Service Management*, vol. 18, no. 4, pp. 4829-4845, Dec. 2021, doi: 10.1109/TNSM.2021.3106577.
- [4] S. Elhoushy, M. Ibrahim and W. Hamouda, "Cell-Free Massive MIMO: A Survey," *IEEE Communications Surveys & Tutorials*, vol. 24, no. 1, pp. 492-523, Firstquarter 2022, doi: 10.1109/COMST.2021.3123267.
- [5] M. Matthaiou, O. Yurduseven, H. Q. Ngo, D. Morales-Jimenez, S. L. Cotton and V. F. Fusco, "The Road to 6G: Ten Physical Layer Challenges for Communications Engineers," *IEEE Communications Magazine*, vol. 59, no. 1, pp. 64-69, January 2021, doi: 10.1109/MCOM.001.2000208.
- [6] X. Xia et al., "Joint User Selection and Transceiver Design for Cell-Free With Network-Assisted Full Duplexing," *IEEE Transactions on Wireless Communications*, vol. 20, no. 12, pp. 7856-7870, Dec. 2021, doi: 10.1109/TWC.2021.3088485.
- [7] X. You, C.-X. Wang, J. Huang et al. "Towards 6G wireless communication networks: vision, enabling technologies, and new paradigm shifts," *Sci China Inf Sci*, vol. 64, no. 1, pp. 1-74, 2021, doi: 10.1007/s11432-020-2955-6
- [8] J. Fu, P. Zhu, J. Li, Y. Wang and X. You, "Beamforming Design in Short-Packet Transmission for URLLC in Cell-Free Massive MIMO System," *IEEE Systems Journal*, doi: 10.1109/JSYST.2023.3234006.
- [9] Y. Polyanskiy, H. V. Poor and S. Verdú, "Channel Coding Rate in the Finite Blocklength Regime," *IEEE Transactions on Information Theory*, vol. 56, no. 5, pp. 2307-2359, May 2010, doi: 10.1109/TIT.2010.2043769.
- [10] W. Yang, G. Durisi, T. Koch and Y. Polyanskiy, "Quasi-Static Multiple-Antenna Fading Channels at Finite Blocklength," *IEEE Transactions on Information Theory*, vol. 60, no. 7, pp. 4232-4265, July 2014, doi: 10.1109/TIT.2014.2318726.
- [11] J. Xu, L. Yuan, N. Yang, N. Yang and Y. Guo, "Performance Analysis of STAR-IRS Aided NOMA Short-Packet Communications With Statistical CSI," *IEEE Transactions on Vehicular Technology*, doi: 10.1109/TVT.2023.3266830.
- [12] J. Jalali, A. Khalili, A. Rezaei, R. Berkvens, M. Weyn and J. Famaey, "IRS-Based Energy Efficiency and Admission Control Maximization for IoT Users With Short Packet Lengths," *IEEE Transactions on Vehicular Technology*, doi: 10.1109/TVT.2023.3266424.
- [13] S. Han et al., "Energy-Efficient Short Packet Communications for Uplink NOMA-Based Massive MTC Networks," *IEEE Transactions on Vehicular Technology*, vol. 68, no. 12, pp. 12066-12078, Dec. 2019, doi: 10.1109/TVT.2019.2948761.
- [14] C. Feng, H.-M. Wang and H. V. Poor, "Reliable and Secure Short-Packet Communications," *IEEE Transactions on Wireless Communications*, vol. 21, no. 3, pp. 1913-1926, March 2022, doi: 10.1109/TWC.2021.3108042.
- [15] X. Lai, T. Wu, Q. Zhang and J. Qin, "Average Secure BLER Analysis of NOMA Downlink Short-Packet Communication Systems in Flat Rayleigh Fading Channels," *IEEE Transactions on Wireless Communications*, vol. 20, no. 5, pp. 2948-2960, May 2021, doi: 10.1109/TWC.2020.3045736.
- [16] H. Zhu and J. Wang, "Chunk-based resource allocation in OFDMA systems - Part I: chunk allocation," *IEEE Transactions on Communications*, vol. 57, no. 9, pp. 2734-2744, Sept. 2009.
- [17] H. Zhu and J. Wang, "Chunk-based resource allocation in OFDMA systems - Part II: joint chunk, power and bit allocation," *IEEE Transactions on Communications*, vol. 60, no. 2, pp. 499-509, Feb. 2012.
- [18] D. W. K. Ng, E. S. Lo and R. Schober, "Energy-Efficient Resource Allocation in OFDMA Systems with Large Numbers of Base Station Antennas," *IEEE Transactions on Wireless Communications*, vol. 11, no. 9, pp. 3292-3304, September 2012, doi: 10.1109/TWC.2012.072512.111850.
- [19] Y. Sun, D. W. K. Ng, J. Zhu and R. Schober, "Robust and Secure Resource Allocation for Full-Duplex MISO Multicarrier NOMA Systems," *IEEE Transactions on Communications*, vol. 66, no. 9, pp. 4119-4137, Sept. 2018, doi: 10.1109/TCOMM.2018.2830325.
- [20] Y. Sun, D. W. K. Ng, Z. Ding and R. Schober, "Optimal Joint Power and Subcarrier Allocation for Full-Duplex Multicarrier Non-Orthogonal Multiple Access Systems," *IEEE Transactions on Communications*, vol. 65, no. 3, pp. 1077-1091, March 2017, doi: 10.1109/TCOMM.2017.2650992.
- [21] Wireless LAN Medium Access Control (MAC) and Physical Layer (PHY) Specifications: Enhancements for Higher Throughput, *IEEE P802.11n Std.*, Sep. 2009.
- [22] P. Zhu, Z. Sheng, J. Bao and J. Li, "Antenna Selection for Full-Duplex Distributed Massive MIMO via the Elite Preservation Genetic Algorithm," *IEEE Communications Letters*, vol. 26, no. 4, pp. 922-926, April 2022, doi: 10.1109/LCOMM.2022.3141546.
- [23] N. Su et al., "Joint MU-MIMO Precoding and Computation Optimization for Energy Efficient Industrial IoT with Mobile Edge Computing," *IEEE Transactions on Green Communications and Networking*, doi: 10.1109/TGCN.2023.3262647.
- [24] S. Fodor, G. Fodor, D. Gürgünoğlu and M. Telek, "Optimizing Pilot Spacing in MU-MIMO Systems Operating Over Aging Channels," *IEEE Transactions on Communications*, doi: 10.1109/TCOMM.2023.3261384.
- [25] D. Pereira-Ruísánchez, Ó. Fresnedo, D. Pérez-Adán and L. Castedo, "Deep Contextual Bandit and Reinforcement Learning for IRS-Assisted MU-MIMO Systems," *IEEE Transactions on Vehicular Technology*, doi: 10.1109/TVT.2023.3249353.

- [26] S. He, Z. An, J. Zhu, J. Zhang, Y. Huang and Y. Zhang, "Beamforming Design for Multiuser uRLLC With Finite Blocklength Transmission," *IEEE Transactions on Wireless Communications*, vol. 20, no. 12, pp. 8096-8109, Dec. 2021, doi: 10.1109/TWC.2021.3090197.
- [27] B. Liu, P. Zhu, J. Li, D. Wang and X. You, "Energy-Efficient Optimization in Distributed Massive MIMO Systems for Slicing eMBB and URLLC Services," *IEEE Transactions on Vehicular Technology*, doi: 10.1109/TVT.2023.3260988.
- [28] W. R. Ghanem, V. Jamali and R. Schober, "Optimal Resource Allocation for Multi-User OFDMA-URLLC MEC Systems," *IEEE Open Journal of the Communications Society*, vol. 3, pp. 2005-2023, 2022, doi: 10.1109/OJCOMS.2022.3216348.
- [29] W. R. Ghanem, V. Jamali and R. Schober, "Joint Beamforming and Phase Shift Optimization for Multicell IRS-aided OFDMA-URLLC Systems," in *2021 IEEE Wireless Communications and Networking Conference (WCNC)*, Nanjing, China, 2021, pp. 1-7, doi: 10.1109/WCNC49053.2021.9417582.
- [30] J. Cheng, C. Shen and S. Xia, "Robust Resource Allocation for Multi-Antenna URLLC-OFDMA Systems in a Smart Factory," in *2021 IEEE/CIC International Conference on Communications in China (ICCC)*, Xiamen, China, 2021, pp. 404-409, doi: 10.1109/ICCC52777.2021.9580345.
- [31] C. van Rensburg and I. Al Falujah, "Coordinated Massive MIMO with Power Control: An Efficient Solution for MU & SU-MIMO Scheduling," in *2021 IEEE 93rd Vehicular Technology Conference (VTC2021-Spring)*, Helsinki, Finland, 2021, pp. 1-6, doi: 10.1109/VTC2021-Spring51267.2021.9449070.
- [32] X. Gong and G. Wu, "Dynamic User Scheduling with User Satisfaction Rate in Cell-Free Massive MIMO," in *2022 IEEE/CIC International Conference on Communications in China (ICCC Workshops)*, Sanshui, Foshan, China, 2022, pp. 100-105, doi: 10.1109/ICCCWorkshops55477.2022.9896715.
- [33] M. Soleymani, I. Santamaria, E. Jorswieck and S. Rezvani, "NOMA-Based Improper Signaling for Multicell MISO RIS-Assisted Broadcast Channels," *IEEE Transactions on Signal Processing*, vol. 71, pp. 963-978, 2023, doi: 10.1109/TSP.2023.3259145.
- [34] L. Schynol and M. Pesavento, "Coordinated Sum-Rate Maximization in Multicell MU-MIMO With Deep Unrolling," *IEEE Journal on Selected Areas in Communications*, vol. 41, no. 4, pp. 1120-1134, April 2023, doi: 10.1109/JSAC.2023.3242716.
- [35] G. Interdonato, S. Buzzi, C. D'andrea, L. Venturino, C. D'elia and P. Vendittelli, "On the Coexistence of eMBB and URLLC in Multi-Cell Massive MIMO," *IEEE Open Journal of the Communications Society*, doi: 10.1109/OJCOMS.2023.3266581.
- [36] W. R. Ghanem, V. Jamali, Y. Sun and R. Schober, "Resource Allocation for Multi-User Downlink MISO OFDMA-URLLC Systems," *IEEE Transactions on Communications*, vol. 68, no. 11, pp. 7184-7200, Nov. 2020, doi: 10.1109/TCOMM.2020.3017757.
- [37] T. Zhang, S. Wang, Y. Zhuang, C. You, M. Wen and Y. -C. Wu, "Reconfigurable Intelligent Surface Assisted OFDM Relaying: Sub-carrier Matching With Balanced SNR," *IEEE Transactions on Vehicular Technology*, vol. 72, no. 2, pp. 2216-2230, Feb. 2023, doi: 10.1109/TVT.2022.3213368.
- [38] P. Wang et al., "Analysis of Rateless Multiple Access Scheme with Maximum Likelihood Decoding in an AWGN Channel," *IEEE Transactions on Wireless Communications*, doi: 10.1109/TWC.2022.3232781.
- [39] E. Che, H. D. Tuan and H. H. Nguyen, "Joint Optimization of Cooperative Beamforming and Relay Assignment in Multi-User Wireless Relay Networks," *IEEE Transactions on Wireless Communications*, vol. 13, no. 10, pp. 5481-5495, Oct. 2014, doi: 10.1109/TWC.2014.2324588.
- [40] X. You, D. Wang, and J. Wang, *Distributed MIMO and Cell-free Mobile Communication*. Springer, 2021.